This is a postprint version of the published document at:

Raiola, M., Greco, C. S, Contino, M., Discetti, S. y Ianiro, A. (2017). Towards enabling time-resolved measurements of turbulent convective heat transfer maps with IR thermography and a heated thin foil. *International Journal of Heat and Mass Transfer*, 108, Part A, pp. 199-209.

DOI: https://doi.org/10.1016/j.ijheatmasstransfer.2016.12.002

Towards enabling time-resolved measurements of turbulent convective heat transfer maps with IR thermography and a heated thin foil

Marco Raiola[a], Carlo Salvatore Greco[b], Mattia Contino[b], Stefano Discetti[a], Andrea Ianiro*[a]

[a]Aerospace Engineering Group, Universidad Carlos III de Madrid, Leganés, Spain

[b]Dipartimento di Ingegneria Industriale, Universitá degli Studi di Napoli Federico II, Napoli, Italy

*-corresponding author: aianiro@ing.uc3m.es

Abstract The temperature of a heated foil, exposed to a turbulent flow, changes continuously in time due to the fluctuation of the convective heat transfer coefficient. Measuring with enough temporal resolution the foil temperature map and solving the unsteady energy balance of the foil can allow restoring the instantaneous value of the convective heat transfer coefficient. Nevertheless, the high characteristic frequencies of turbulent flows (especially in air) result in very small temperature fluctuations, which are typically hard to measure with an infrared camera. This work presents a novel filtering approach based on Proper Orthogonal Decomposition which allows to dramatically reduce the measurement random noise, thus enabling the detection of small temperature fluctuations and, as a consequence, to improve the estimate of instantaneous distributions of the convective heat transfer coefficient.

The proposed methodology is tested on synthetic jets impinging on a foil, actuated with a loudspeaker at various actuation frequencies. The measurement capability of the present technique is assessed through comparison with measurements obtained from raw data and phase averaged measurements.

Keywords: Unsteady flows, Low order modelling, Proper Orthogonal Decomposition, Convective heat transfer, Infrared thermography

Nomenclature

Roman letters

Bi	Biot number
c	Specific heat coefficient
C	Constant of integration
D	Exit diameter of the nozzle
$\underline{E}$	Random error
f	Characteristic frequency
f_A	Actuation frequency of the synthetic jet
$F(k)$	Function to evaluate relative importance of modes until k
Fo	Modified Fourier number
h	Convective heat transfer coefficient
$\underline{\underline{I_j}}$	Rank j identity matrix
k	Thermal conductivity
$k^\star$	Optimum number of modes
l_i	Eddy characteristic wavelength
L_0	Stoke length of the synthetic jet
n	Number of samples
Nu	Nusselt number
p	Number of grid points
q	Variance of the temperature fluctuation
q_{cv}	Convective heat flux
q_j	Heat flux input
q_k	Tangential conduction heat flux
q_r	Radiation heat flux
Sr	Strouhal number
r	Radial coordinates over the heated thin foil
Re	Reynolds number
RF	Noise reduction factor
t	Time
T_{aw}	Adiabatic wall temperature
T_{amb}	Ambient temperature
T_w	Wall temperature
x, y	Cartesian coordinates over the heated thin foil
u_a	Nozzle exit axial velocity on the jet axis
U_0	Characteristic velocity of the jet
$\underline{\underline{U}}, \underline{\underline{V}}$	Decomposition basis of the fluctuating temperature field $\underline{\underline{\Delta T}}$

Greek letters

β	Stefan-Boltzmann constant
δ	Thickness of the heated thin foil
$\delta_{RM}(k)$	Reconstruction error with respect to the measured temperature field taking into account an arbitrary number of modes k
$\delta_{RT}(k)$	Reconstruction error with respect to the true temperature field taking into account an arbitrary number of modes k
ε	Wall material emissivity
ζ	Euler-Riemann zeta function
λ_i	Eigenvalue of the two point temporal correlation matrix of

	temperature fluctuations
μ	Dynamic viscosity
ν	Kinematic viscosity
ρ	Density
σ_{IR}	Time standard deviation of the random background noise in the IR images
$\underline{\underline{\Sigma}}$	Diagonal matrix containing singular values
τ	Actuation period of the synthetic jet $= 1/f_A$

Other symbols

$\widetilde{\underline{\underline{\Delta()}}}$	Measured field
$\overline{\underline{\underline{\Delta()}}}$	Fluctuating field
$()_e$	Quantity referred to random error
$()_k$	Reconstruction to the k most relevant modes
$()^*$	Complex conjugate
$\mathbb{R}$	Set of real number
∇^2	Laplacian operator
$Tr()$	Trace operator

Acronyms

IR	InfraRed
LOR	Low Order Reconstruction
NETD	Noise Equivalent Temperature Difference
PIV	Particle Image velocimetry
POD	Proper Orthogonal Decomposition

1. Introduction

The intrinsic unsteadiness and the three-dimensionality of turbulent flows challenges measurement capabilities when dealing with turbulent convective heat fluxes. Measuring heat fluxes in thermo-fluid-dynamics requires both a heat-flux sensor (with its related thermo-physical model) and temperature transducers. Fast temporal response can be achieved, for example, using thin film gauges or coaxial thermocouples, sacrificing, on the downside, the spatial resolution. Infrared (IR) cameras constitute a truly two-dimensional non-intrusive temperature transducer which allows to accurately measure (thermal resolution down to $10mK$) surface temperatures at high resolutions (up to $1\ Mpixel$) and high repetition rate (up to $1.5kHz$ at ambient temperature), thus being a promising candidate for time-resolved turbulent convective heat transfer investigations.

The combined use of IR thermography and a heated thin foil heat transfer sensor has been widely assessed for two-dimensional time-averaged heat transfer measurements (see e.g. the review articles [1],[2]) and researchers have enjoyed these capabilities in several fields of thermo-fluid dynamics. Nevertheless, time-averaged measurements are not able to uncover the important aspects related to the dynamics of turbulent flows, thus not allowing to fully disclose the underlying physics.

Few studies have dealt with the measurements of unsteady heat transfer maps, being notable examples the works by Hetsroni and Rozenblit [3] on a liquid-solid mixture in a flume, Sanmiguel Vila et al. [4] on horizontal convection in water, Greco et al. [5] who performed phase averaged measurements on synthetic jets in air and Nakamura and Yamada [6] who performed time-resolved measurements on a turbulent boundary layer over a flat plate in a wind tunnel. More recently, Yamada and Nakamura [7] performed similar measurements on a backward facing step. To the authors' knowledge, [6] and [7] represent to date the only successful experiments dealing with time resolved heat transfer measurements in air using optical thermography.

The reasons of such a limited number of experiments are well described in the seminal work by Nakamura [8] which shows that the fluctuations in the temperature distribution over a foil immersed in a turbulent flow are attenuated in space due to the foil thermal conductivity and in time due to the foil thermal inertia.

In fact, consider the energy balance of a heated thin foil as sketched in Figure 1,

$$c\rho\delta \frac{dT_w}{dt} = q_j + k_{foil}\delta\nabla^2 T_w - h(T_w - T_{aw}) - \varepsilon\beta(T_w^4 - T_{amb}^4) \qquad (1)$$

in which c, ρ, k_{foil} and δ are respectively the specific heat coefficient, the density, the thermal conductivity and the thickness of the heated thin foil, q_j is the input heat flux (typically given by Joule effect and assumed for simplicity being spatially uniform), h is the convective heat transfer coefficient, T_w and T_{aw} are respectively

the wall temperature and the adiabatic wall temperature, ε is the wall material emissivity, β is the Stefan-Boltzmann constant and T_{amb} is the ambient temperature. The last three contributions on the right hand side of the equation are indicated, respectively, with the symbols q_k, q_{cv} and q_r, and represent the heat transfer contributions due to tangential conduction, forced convection and radiation. The wall temperature T_w is assumed to be constant through the foil thickness and the heat transfer on the foil side which is not interested by the turbulent flow is considered as negligible. The first assumption is verified if the Biot number $Bi = h\delta/k_{foil}$ is much smaller than unity and the modified Fourier number $Fo = k_{foil}/(\rho c \pi f \delta^2)$ is much greater than one, i.e. the characteristic period $1/f$ of the observed phenomenon is much greater than the characteristic time of heat diffusion through the foil [9].
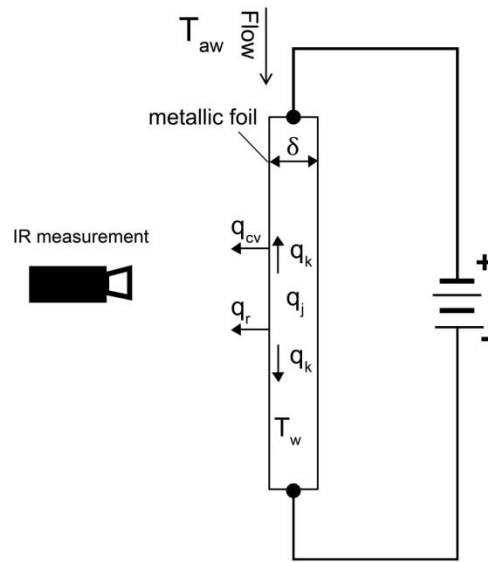

Figure 1 Heated thin foil energy balance.

If the frequency of the observed phenomenon is sufficiently large [8], the temperature fluctuation attenuation is directly proportional to the convective heat transfer fluctuations frequency and almost inversely proportional to the square of the spatial wavelength of the fluctuation. Easily, the temperature fluctuations can fall below the thermal resolution of the IR camera. This explains why most of the successful unsteady heat transfer measurements have been performed in water where the flow speed (and thus temporal frequencies) is much smaller than in air for the same Reynolds number. Successful experiments in air have been performed on phase-averaged signals (in which the temperature accuracy of the camera is increased through the averaging process) by Greco et al. [5] and on very thin foils (which reduce the foil thermal inertia) in [6] and [7].

Although being more difficult to handle and less practical than the $50\mu m$ foils used for typical experiments in air, foils with few micron thickness represent a suitable solution for the measurements of large-scale turbulent fluctuations. Nevertheless, Nakamura [8] reports that a $2\mu m$ thick titanium foil could track a maximum frequency of $35Hz$ in a typical experiment in air performed by heating the plate of $30K$ and considering turbulent structures with a typical convective heat transfer coefficient $\Delta h = 5\frac{W}{m^2 K}$. For this reason in Nakamura and Yamada [6] it is reported that data are additionally *cleaned* with a low-pass filter in space and time. Considering the case of a transitional (Reynolds number of the order of 2000) impinging air jet with a diameter of $1cm$, even a very thin foil would clearly not be able to track temperature fluctuations related to the large scale ring vortices developed in the shear layer which would have a typical Strouhal number of order 1 i.e. would have a temporal frequency of the order of $100Hz$.

Owing to the large spectral distribution of turbulent flows, the different modulation pertaining to such frequencies due to the foil thermal inertia and the low level of the temperature fluctuations intensity, the filtering of the data is a challenging task and requires proper tuning. Raiola et al. [10] proposed an approach based on the use of Proper Orthogonal Decomposition (POD) as a statistical filter [11] of velocity data ensembles to reduce significantly the noise contamination of Particle Image Velocimetry (PIV) measurements. POD allows for the identification of the principal components of the measured flow fields, providing an optimal (with respect to the turbulent kinetic energy) description of the flow phenomenology. A Low-Order Reconstruction (LOR) obtained using a limited subset of modes acts as a filter on the data while, at the same time, redistributes information from the entire ensemble into the single snapshots. Raiola et al. [10] have demonstrated that such a filter is capable of dramatically increasing the measurements dynamic range and enables improving the accuracy when measuring PIV spectra at high frequency (which is not possible with a low pass filter). The POD-based filter is, practically, flow-feature oriented rather than signal-oriented. In the same work, a criterion to identify the optimal number of modes to be used in order to minimize the loss of signal while at the same time maximizing the noise removal was proposed and assessed.

In this paper, we propose to apply the approach proposed in [10] to IR camera temperature measurements of a heated thin foil immersed in a turbulent flow. The objective is to reduce dramatically the IR camera noise which affects temperature measurements in order to increase the range of wavelengths and frequencies which can be correctly detected by an IR sensor. Approaches based on POD have already been shown to be successful in de-noising of imaging techniques (see for example the POD-based filtering of pressure sensitive paint data in [12]), even though the selection of the optimal number of modes is often based on the user sensitivity or on energy-recovery principles (i.e. using the number of modes including a certain percentage of the energy of the signal).

The method is presented in detail in section 2, where the theoretical background of unsteady heat transfer measurements with IR thermography and the fundamentals of the POD based filter are outlined. The technique is assessed in section 3 by applying it to turbulent synthetic impinging jets actuated with a loudspeaker at various actuation frequencies.

2. Methodology and theoretical background

2.1 Unsteady heat transfer measurements with infrared thermography

The implementation of the heated thin foil heat transfer sensor (Eq. 1) to obtain convective heat transfer maps requires the field measurement of the surface temperature of the sensor. This has pushed towards the extensive use of IR cameras to accomplish this task. The core of an IR camera sensor is the thermal detector, i.e. the element which integrates over a certain time the thermal radiation received and converts it into an electrical signal. Among the several performance parameters qualifying an infrared scanner, the most relevant when performing time-resolved heat flux measurements are the acquisition frequency and the thermal sensitivity. The acquisition frequency should be large enough to adequately sample the observed phenomena; this condition is typically satisfied in low speed flows since high performance sensors can achieve an integration time as low as $500\mu s$ at ambient temperature and even lower at higher temperatures. The thermal sensitivity is generally quantified in terms of noise equivalent temperature difference (NETD), which is the standard deviation of the random background noise over all the pixels when imaging a black body at uniform and constant temperature [13]. The IR camera manufacturer typically quantifies the NETD at ambient temperature (even though it depends on the temperature of the black body itself), with figure of merit of modern scanners down to values of the order of $10mK$.

As anticipated in the introduction, in order to resolve the relatively small temperature fluctuations of the unsteady convective heat transfer of turbulent flows, it is required that those fluctuations in time are sufficiently larger than the NETD, otherwise they will be inevitably overwhelmed by the noise. Under the same assumptions of Eq. 1, this requirement is translated as:

$$\frac{k_{foil}\delta\nabla^2 T_w + q_j - h(T_w - T_{aw}) - \varepsilon\beta(T_w^4 - T_{amb}^4)}{c\rho\delta f \sigma_{IR}} \gg 1 \qquad (2)$$

where f is the characteristic frequency of the temperature temporal fluctuations to be measured and σ_{IR} is the time standard deviation of the random background noise in the IR images (thus, starting from the raw images, is the NETD of the scanner, intended as the standard deviation of the noise experienced pixel-wise over time). While the characteristic thermal diffusion time through the foil is typically very small and the assumption of modified Fourier number $Fo =$

$k_{foil}/\pi\rho c f \delta^2 \gg 1$ is almost always verified, the thermal inertia of the foil $c\rho\delta$ greatly challenges the achievement of the requirement of Eq. 2.

The cut-off frequency for the measurement can be enhanced by tampering with some of the experimental parameters. It has been discussed in the introduction that several authors have satisfied the requirement in Eq. 2 by reducing the foil thickness or by dealing with slower flows in water (thus reducing f) either by reducing the effect of σ_{IR} by performing phase averages (thus retaining only information on the largest scales of turbulence).

In this work it is proposed to reduce σ_{IR} over instantaneous images by filtering the data with a POD-based low order reconstruction as described in detail in the next subsection.

2.2 POD-based filter for temperature maps noise reduction

The Proper Orthogonal Decomposition is a mathematical procedure that identifies an orthonormal basis using functions estimated as solutions of the integral eigenvalue problem known as Fredholm equation (see [14] for a rigorous formulation).

Consider a data matrix, that for the case of IR thermography measurements is the sample ensemble of the fluctuating part of the temperature field, $\underline{\underline{\Delta T}} \in \mathbb{R}^{n \times p}$, where n is the number of samples and p is the number of grid points. $\underline{\underline{\Delta T}}$ can be decomposed as:

$$\underline{\underline{\Delta T}} = \underline{\underline{U}}\,\underline{\underline{\Sigma}}\,\underline{\underline{V}}^*$$
(3)

where $\underline{\underline{U}}$ and $\underline{\underline{V}}$ constitute the decomposition basis of the fluctuating temperature field $\underline{\underline{\Delta T}}$, respectively in space and time, and $\underline{\underline{\Sigma}}$ is a diagonal matrix containing the singular values associated to the fluctuating field. It can be shown that this decomposition is intimately related to the POD. The snapshots method proposed by Sirovich [15] assumes that the POD modes are calculated as the eigenmodes of the two-point temporal correlation matrix. The snapshot method provides a base composed of a number of eigenfunctions (i.e. spatial modes) equal to that of the snapshots.

The Singular Value Decomposition procedure provides modes which are sorted by descending singular values, representative of the contribution of each mode to the temperature fluctuating intensity (i.e. variance). This allows to reconstruct the field by truncating the reconstruction to the k most relevant modes (in terms of variance):

$$\underline{\underline{\Delta T_k}} = \underline{\underline{U}} \begin{pmatrix} \underline{\underline{I_k}} & 0 \\ 0 & 0 \end{pmatrix} \underline{\underline{\Sigma}}\,\underline{\underline{V}}^*$$
(4)

where $\underline{\underline{\Delta T_k}}$ is the reconstructed fluctuating temperature field, $\underline{\underline{I_k}}$ indicates the rank k identity matrix and 0 indicates that the matrix containing $\underline{\underline{I_k}}$ is a square matrix of dimension $n \times n$ with zero entries except for I_k.

A qualitative argument on the existence of an optimum value of k for the suppression of noise from a set of IR images can be easily derived if we consider the measured field $\underline{\underline{\widetilde{\Delta T}}}$ as the sum of an objective fluctuating field $\underline{\underline{\Delta T}}$ (that is the measured field in absence of random errors) and of a measurement random error $\underline{\underline{E}}$ (noise). For statistically uncorrelated noise it can be demonstrated that:

$$\underline{\underline{\widetilde{\Delta T}_k}} = \underline{\underline{\Delta T_k}} + \underline{\underline{E_k}} \approx \underline{\underline{U}} \begin{pmatrix} \underline{\underline{I_k}} & 0 \\ 0 & 0 \end{pmatrix} \left(\underline{\underline{\Sigma}} + \underline{\underline{\Sigma}}_e \right) \underline{\underline{V}}^* \tag{5}$$

where $\underline{\underline{\Sigma}}_e = \underline{\underline{U}}^* \, \underline{\underline{E}} \, \underline{\underline{V}}$.

The true fluctuating temperature field should have a singular values distribution that asymptotically goes to zero, as the bulk of temperature variance should be ascribed to the largest coherent structures (as asserted in [11] for the case of POD analysis of velocity fields). The measurement random error (that is spatially and temporally uncorrelated) should have a nearly uniform distribution of singular values all over the POD modes. In practice, the measurement random error is expected to behave spectrally like a white noise. As a consequence, an optimum number of modes $k^\star$ can be identified beyond which the variance content of noise added by the subsequent mode is equal or higher than that of the real signal. Dropping all the following modes after this $k^\star$ will ensure that the variance of discarded real temperature fluctuations is lower than the variance of the discarded noise.

The reconstruction error δ_{RT} with respect to the true temperature field is defined as:

$$\delta_{RT}(k) = \left(\frac{1}{np} Tr \left(\left(\underline{\underline{\Delta T}} - \underline{\underline{\widetilde{\Delta T}_k}} \right) \left(\underline{\underline{\Delta T}} - \underline{\underline{\widetilde{\Delta T}_k}} \right) \right) \right)^{0.5} \tag{6}$$

which is of course unknown when performing an experiment, thus a direct evaluation of the optimum $k^\star$ via minimization of $\delta_{RT}(k)$ is not possible.

A simplified model to predict the order of magnitude of $k^\star$ for the case of velocity fields' reconstruction via POD is reported in [10]. The model is based on the assumption that, due to the variance optimality of the POD, i.e. the property of POD to maximize the variance content of each mode, the POD eigenvalues should decay faster than any other spectral representation, and consequently faster than the -5/3 decay of the turbulent kinetic energy in the inertial subrange of turbulent flows [16].

A similar argument is developed here for the case of temperature fluctuations due to turbulent convective heat transfer. Consider the turbulent flow field as

composed of several eddies, each one with its own wavelength, corresponding to a certain frequency equal to the eddy convection velocity (of the order of the free stream velocity) divided by its wavelength. Provided that the frequency is sufficiently large [8], the fluctuating temperature due to a certain i^{th} eddy decreases (increases) linearly with its frequency f_i (wavelength l_i), and increases linearly with the fluctuating convective heat transfer coefficient due to that eddy. If the eddy's Reynolds number $Re_{l,i} = u_i l_i / \nu$ is sufficiently small (being ν the kinematic viscosity and u_i the eddy's fluctuating velocity) it can be assumed that the Nusselt number relative to the eddy is proportional to the square root of $Re_{l,i}$, thus it is possible to write that:

$$\Delta T_i \propto \frac{h_i}{f_i} = \frac{kNu_i}{l_i f_i} \propto \sqrt{Re_{l,i}} = \sqrt{\frac{u_i l_i}{\nu}} \tag{7}$$

In the inertial subrange the velocity scale is uniquely determined by the dissipation rate, thus it has to scale with $l_i^{1/3}$ [16]. This means that temperature fluctuation intensity $o(\Delta T^2)$ is proportional to $l^{4/3}$.

Assuming that the random error behaves spectrally as a white noise and that the real signal contribution decreases with increasing number of modes it is possible to write that:

$$Tr\left(\left(\underline{\underline{\Delta T}} - \underline{\underline{\widetilde{\Delta T}_k}} \right) \left(\underline{\underline{\Delta T}} - \underline{\underline{\widetilde{\Delta T}_k}} \right) \right) = kp\sigma_{IR}^2 + \sum_{i=k+1}^{n} \lambda_i \tag{8}$$

where σ_{IR} is the IR camera noise standard deviation and λ_i are the eigenvalues of the two point temporal correlation matrix of temperature fluctuations. According to Eq. 7, assuming that the wavelength decreases with the number of modes i, for experimental data of turbulent flows it can be written that $\lambda_i = C \cdot l^{4/3} = C \cdot i^{-4/3}$ where C is a constant. To evaluate it, one can consider that the sum of the eigenvalues λ_i is equal to the total temperature variance of the ensemble:

$$\sum_{i=1}^{n} \lambda_i = \sum_{i=1}^{n} C i^{-4/3} = npq \rightarrow C = \frac{npq}{\zeta(4/3)} \tag{9}$$

where q is the variance of the temperature fluctuation and $\zeta(4/3)$ is the Euler-Riemann zeta function of $4/3$.

The order of magnitude of the optimal number of modes to be retained $k^\star$ can be calculated from Eq. 10 by discrete deriving δ_{RT} with respect to k and equating to zero:

$$k^\star \approx \left(\frac{n\,q}{\sigma_{IR}^2 \zeta\left(\frac{4}{3}\right)}\right)^{\frac{3}{4}} \qquad (10)$$

Considering a white spectrum for the random error (thus assuming that the error equally contributes to all modes), the number of statistically independent snapshots n to be used in the decomposition in order to achieve a certain level of noise reduction can be estimated with Eq. 11:

$$n \approx (1 - RF)^{-4} \left(\frac{q}{\sigma_{IR}^2 \zeta\left(\frac{4}{3}\right)}\right)^3 \qquad (11)$$

where RF is the noise reduction factor (i.e. the residual error fraction in terms of variance of the reconstructed fields is $[1 - RF]\sigma_{IR}^2$).

In IR measurements, the value of σ_{IR} is typically known, or it can be estimated as the pixel-wise NETD of the IR camera, thus $k^\star$ and the number of samples can be computed a priori by estimating the standard deviation of the temperature fluctuations and setting the desired noise reduction factor RF. However, Eq. 10 is the result of approximating the temperature fluctuations with a scaling based on dimensional arguments valid only in the inertial subrange. In order to estimate $k^\star$ in a more robust way, the scree test plot [17] is better suited. The method is based on reconstructing the temperature fields with different number of modes, and then comparing the reconstructed fields with the measured ones, thus obtaining a reconstruction error:

$$\delta_{RM}(k) = \left(\frac{1}{np} Tr\left(\left(\widetilde{\underline{\underline{\Delta T}}} - \underline{\underline{\Delta T_k}}\right)\left(\widetilde{\underline{\underline{\Delta T}}} - \underline{\underline{\Delta T_k}}\right)\right)\right)^{0.5} \qquad (12)$$

$\delta_{RM}(k)$ is a monotonically decreasing function of the number of modes used for the reconstruction and it is equal to 0 for $k = n$. If the kth mode predominantly contains noise, the function $F(k)$, defined as

$$F(k) = \frac{\delta_{RM}^2(k+1) - \delta_{RM}^2(k)}{\delta_{RM}^2(k) - \delta_{RM}^2(k-1)} \qquad (13)$$

will eventually have an asymptote to 1, which is equivalent to say that the modes contribution in building up the variance of the reconstructed temperature fields is linear with k, and thus it approximates well a white spectral distribution.

In the next section, the threshold to identify the optimal number of modes will be set to $F(k^\star) = 0.999$. Notice that this is formally equivalent to searching for an elbow of the function $\delta_{RM}(k)$, which is analogous to the classic scree test plot [17] used in Principal Component Analysis for low order reconstruction algorithms.

3. Application to loudspeaker actuated synthetic impinging jets

11

3.1 Experimental setup

The schematic representation of the experimental apparatus is shown in Figure 2. It consists of a constantan foil impinged by a synthetic jet actuated by a loudspeaker. The constantan foil ($200mm$ wide, $450mm$ long and $50\mu m$ thick) is steadily (in time) and uniformly (in space) heated by Joule effect. The shortest sides of the foil are clamped by two couples of bus bars made of copper. Through these bars, a steady voltage difference is applied by using a stabilized DC power supply producing an input heat flux through Joule effect. Values of heat flux input are reported in Table 1 and are estimated from voltage and current passing through the foil which are measured with two multimeters with 1% uncertainty.

The foil is located at 2 diameters below the synthetic jet exit, which impinges vertically on its top face; this arrangement is chosen in order minimize the effects of natural convection on the measurement accuracy.

The synthetic jet, as sketched in Figure 2, is obtained with a loudspeaker connected to a cavity which periodically ejects and injects air from a nozzle and substantially coincides with the device employed and already well characterized in [18]. The cavity volume V of $2 \cdot 10^{-3} m^3$ is confined by a loudspeaker with a frame diameter of $270mm$. The employed loudspeaker is a CIARE HS250 characterized by a free-space resonance frequency of $25Hz$, a nominal diameter of $208mm$ and an equivalent oscillating mass of $56g$. A pipe with a length L equal to $210mm$ and an inner diameter D of $21mm$ connects the cavity volume to the external ambient.
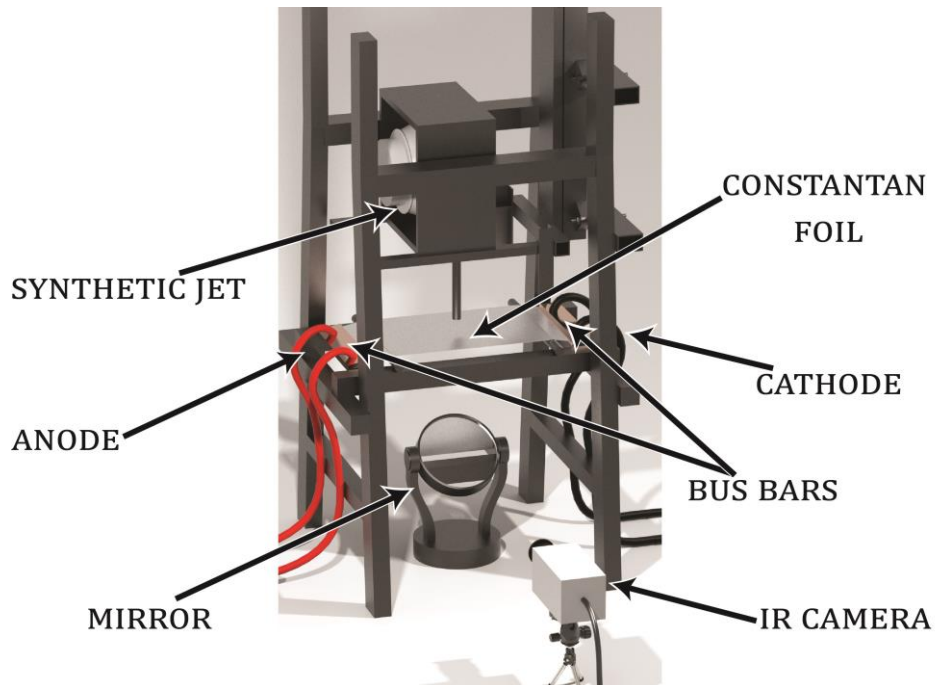

Figure 2 Sketch of the magnified view of the jet arrangement.

The experiments are carried out feeding the loudspeaker with a sinusoidal signal generated by means of an Analog Discovery™ signal generator and amplified through an Hi-Fi amplifier (Kenwood KAC-6405). Three input signals are

generated with a frequency f_A equal to 8, 16 and $32Hz$ and different input voltage. These conditions allow generating three synthetic jets characterized by Strouhal numbers equal to 0.04, 0.08 and 0.16 at the same Reynolds number equal to 5,100. Reynolds number (Eq. 14) and Strouhal number (Eq. 15) are defined as:

$$Re = \rho U_0 D / \mu \tag{14}$$

$$Sr = D / L_0 = f_A D / U_0 \tag{15}$$

where U_0 is the characteristic velocity of the jet, D is the exit diameter, f_A is the actuation frequency, ρ is the air density, μ is the air dynamic viscosity and L_0 is the stroke length (defined as U_0 / f_A). The characteristic velocity, according to [19], is estimated over the ejection part of the synthetic jet cycle and is defined as:

$$U_0 = \frac{1}{\tau} \int_0^{\frac{\tau}{2}} u_a(t) \, dt \tag{16}$$

where $\tau = 1/f_A$ is the actuation period and u_a is the nozzle exit axial velocity on the jet axis. This velocity is measured with a Pitot tube, as in [20], located at the centre of the nozzle exit and connected to a Honeywell differential pressure transducer $(-500 \div 500 \, Pa)$ with accuracy equal to 1.5% of the full scale.

An IR camera (CEPID JADE III 320x240 focal plane array with germanium lens with focal length equal to $25mm$) is used to measure the foil surface temperature with a spatial resolution of $0.76 \, pixels/mm$ ($16 \, pixels/D$). A high-quality-finishing first-surface mirror (with reflectivity equal to 0.98) is placed in the optical path at 45° angle in order to allow for proper camera arrangement. The focal plane array is cropped to a resolution $160x120 \, pixels$ in order to reach sampling frequencies f_s up to $480Hz$ as reported in Table 1 while the integration time is kept equal to $580\mu s$ for all experiments. The calibration of the IR camera is performed with a blackbody according to the procedure described in [9]. The error from the blackbody calibration is less than $0.1K$. The standard deviation of the pixel-wise temperature noise of the camera is estimated to be about $18mK$. The square of the temperature noise is subtracted to the variance of the temperature fluctuation evaluated on the plate at 2 diameters distance from the jet axis, to provide a first-order estimation of the mean square temperature fluctuations for the three experiments, resulting, as expected, in a value decreasing with increasing frequency.

In order to increase the accuracy of the temperature measurements, the rear surface of the foil is coated with a few microns thin layer of high emissivity enamel (ε = 0.95). It has to be remarked that due to its small heat capacity the thermal inertia effects due to the thin paint layer are neglected in this work. In general, neglecting the paint layer thermal inertia would lead to a large measurement error when using thinner foils.

The Nusselt number is computed from equation 1 as:

$$Nu = \frac{D}{k_{air}} \cdot \frac{q_j + k_{foil}\delta\nabla^2 T_w - c\rho\delta\frac{dT_w}{dt} - \varepsilon\beta(T_w^4 - T_{amb}^4)}{(T_w - T_{aw})} \qquad (17)$$

T_w and T_{aw} are measured respectively with the Joule heating on and off. Being the flow incompressible and being the ambient at constant temperature, T_{aw} is practically constant in time and equal to ambient temperature T_{amb}. The temperature measured with Joule heating on T_w is instead found to fluctuate over time and is discussed in the next section.

Re	Sr	$\frac{L_0}{D}$	Actuation frequency [Hz]	Sampling frequency [Hz]	q_j [W/m^2]	Number of images	rms temperature fluctuation [mK]
5,100	0.04	24	8	240	443	6000	25
5,100	0.08	12	16	480	448	6000	19
5,100	0.16	6	32	480	464	3000	17

Table 1 Synthetic jet operating conditions

14

3.2 Results

The rms temperature fluctuations reported in Table 1 can be used for a first order estimation of the number of modes to optimally filter the datasets of the three considered experimental campaigns. In particular, according to Eq. 10, considering an IR camera random noise of $18mK$, the optimal number of modes to be retained is equal to 364, 241 and 121 for the experiments with the synthetic jet actuated at 8, 16 and $32Hz$, respectively. This preliminary estimation needs to be contrasted with the scree plot criterion of Eq. 13. The results of the scree plot are reported in Figure 3 where the optimum number of modes to be retained corresponds to that at the intersection between the F-curve and the dashed horizontal line at $F = 0.999$. Although the results of Eq. 10 provide a good preliminary estimation of k^*, the deviation of the actual data from these values suggests to always use the scree plot criterion to determine the optimal number of modes to be used. However, the tendency of decreasing k^* with increasing frequency is confirmed both by the scree plot criterion and Eq. 10.
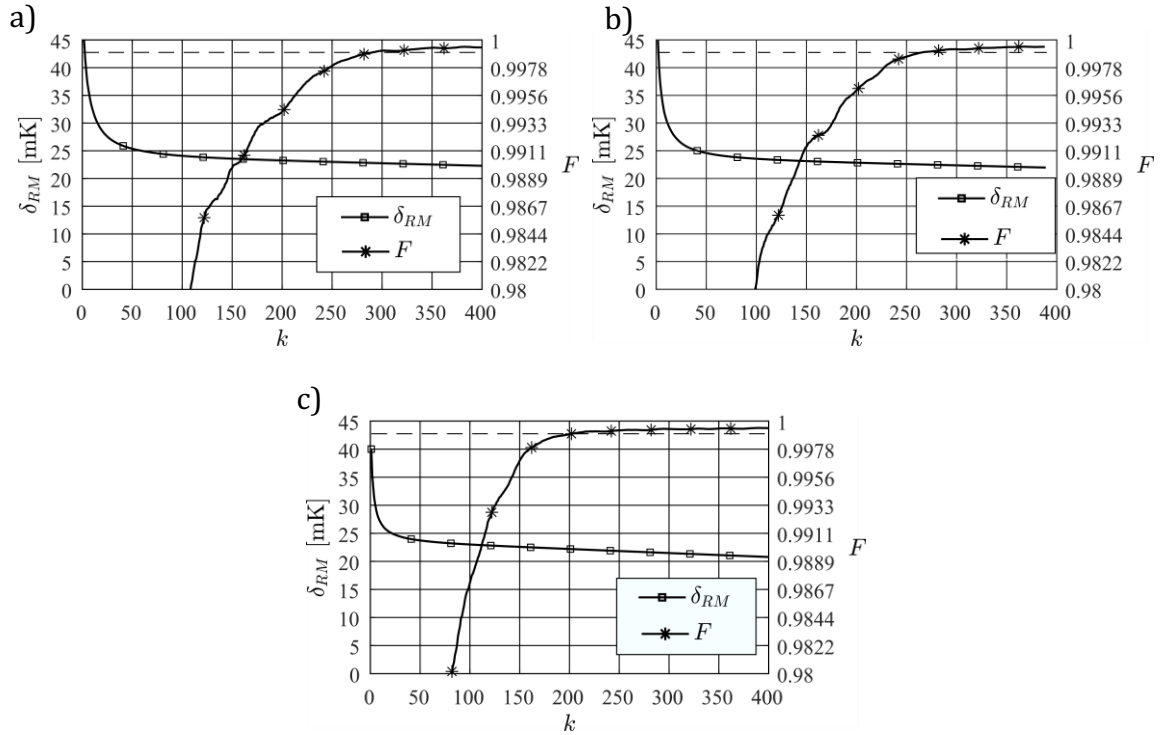
a)

b)

c)

Figure 3 Residual error (Eq. 12) and F parameter variation (Eq. 13) versus number of modes included in the reconstruction: a) $8Hz$ b) $16Hz$ c) $32Hz$.
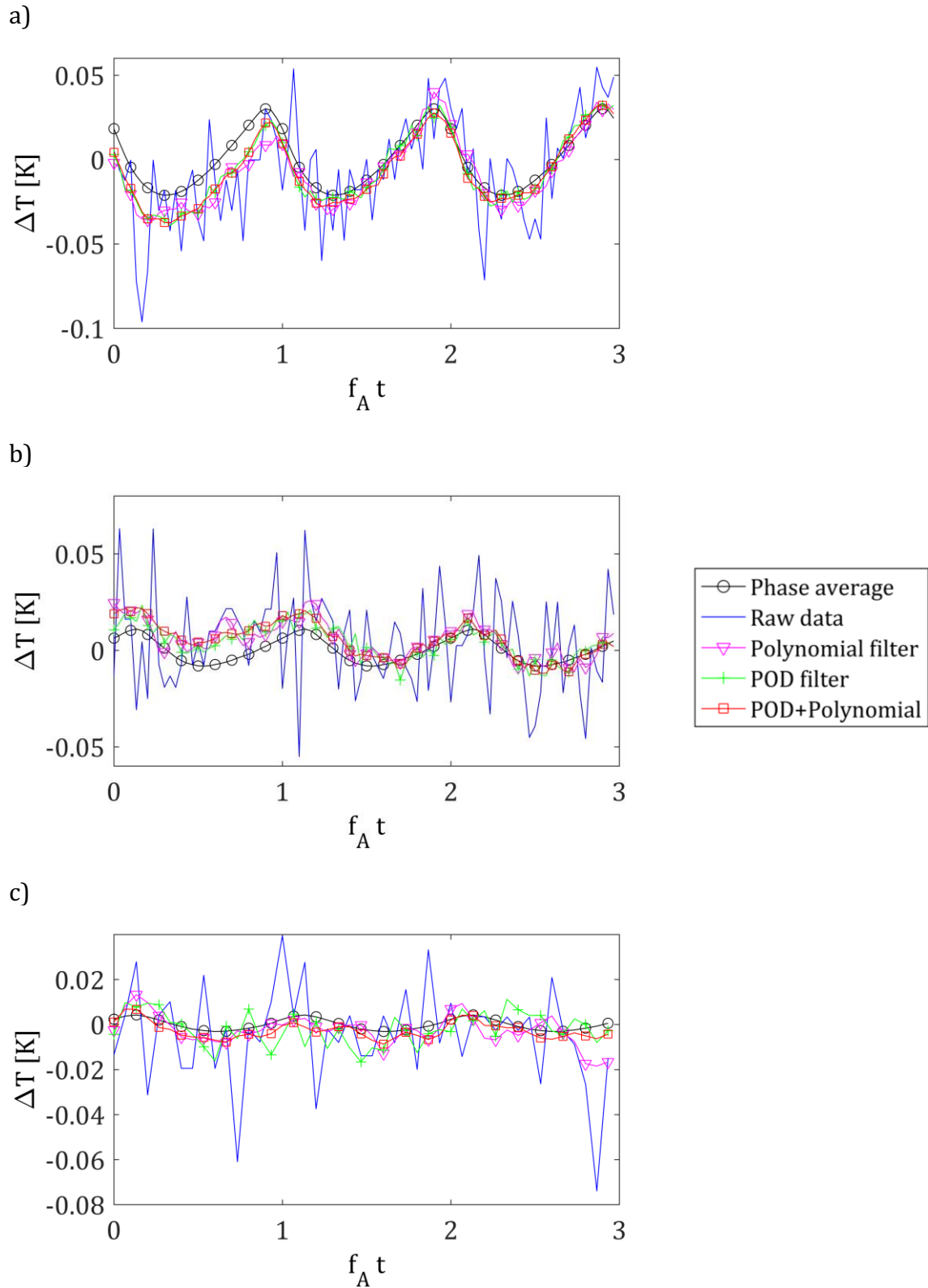
a)

b)

c)

Figure 4 Temporal plot of the fluctuating temperature: a) $8 Hz$ b) $16 Hz$ c) $32 Hz$. Markers are placed each 3 sampled points in (a) and (b), and each 2 sampled points in (c).

Figure 4 reports the temporal evolution of the fluctuating temperature over three jet actuation periods for the same point previously considered for the estimation of

16

the rms temperature fluctuations (located at $x/D = 2, y/D = 0$ of Figure 5-8). The original data are reported against data filtered with a polynomial filter (with a stencil of $5x5\ pixels$ in space and 5 snapshots in time), with the proposed POD filter, with the POD filter plus polynomial filter (same stencil 5x5x5 in space and time) and against phase averaged temperature fluctuations. Naturally, instantaneous temperature differs from the phase averaged one, being the synthetic jet statistically periodic but not fully periodic due to turbulence (see for instance triple decompositions of synthetic impinging jets reported in [21]). As shown in Figure 4, the intensity of the temperature fluctuations to be retained decreases with increasing jet actuation frequency but the proposed POD filter is capable of reducing significantly the camera noise, providing a temperature fluctuation which is closer to the phase average one.

Figure 5, Figure 6 and Figure 7 report the instantaneous map of temperature temporal derivative obtained from the raw temperature data, from the data after applying the polynomial filter, from the data filtered solely through POD and from the temperature data filtered both with POD and polynomial filter. Derivatives are performed with a two-point central derivative stencil. The temporal derivative of the phase averaged temperature is also included for comparison purposes. Independently on the test case, the unfiltered data are overwhelmed by noise, thus can not provide a useful time derivative estimate. For the cases of actuation frequency of $8Hz$ and $16Hz$, respectively in Figure 5 and Figure 6, the polynomial filter can achieve modest result, but still being not capable of providing a clear figure of the instantaneous time derivative distribution. The POD filter, instead, evidently outclasses the polynomial filter in extracting information from the raw data, revealing a clear pattern in the time derivatives. Nevertheless, the POD filter, acting on a statistical level, is not capable of getting rid of the small non-uniformity of the sensor array of the camera (see e.g. [22]). Consequently, even though the POD filter promotes temporal coherence amongst all the sensing elements and the noise level is significantly reduced, residuals of spatial incoherence are still present and would be further amplified in case of spatial derivative computation for the tangential conduction estimation (as discussed in [23]). A further space-time filtering (such as the polynomial filtering) is required in order to regularize the solution, providing a more accurate estimate of the time derivative maps. For the jet at $32Hz$, which represents the most challenging case under examination, temperature fluctuations are very small and are covered by the spatial non-uniformity of the camera response. Applying a polynomial filter on top of the POD filtered data it is possible to extract a clearer estimate of the temperature time derivatives (Figure 7e).

The temperature time derivatives, shown in Figure 5e, Figure 6e and Figure 7e, are deeply influenced by the vortex ring and the trailing jet behavior impinging on the plate. As a matter of fact in Figure 5e, a negative value of dT/dt is clearly visible in a circular region centred on the stagnation point and with a radius of

approximately $1.5D$. This region represents the footprint of the trailing jet which is impinging on the plate whose contribution to the convective heat transfer is positive (see Eq. 1). On the contrary, a wide annular region, outside of this circle, is characterized by positive values of the temperature time derivative. This zone has an opposite contribution to the convective heat transfer because such a region is located ahead of the vortex ring which causes an induced flow field ejecting air away of the impingement plate. It is worth noting that the annular region shows fluctuating values along the azimuthal direction. This azimuthal non-uniformity with radial streaks of lower/higher dT/dt is related to the vortex ring shape which is not perfectly axisymmetric but starts being stretched and tilted due to turbulence; the streaks pattern is randomly distributed if considering samples at the same phase, thus this feature is averaged out in the operation of phase averaging.

The behaviour of the temperature time derivatives for the test at $16Hz$ ($Sr = 0.08$, Figure 6e) shows similar features with respect to the $8Hz$ case (i.e. $Sr = 0.04$). Indeed, this case shows a circular central region with negative values surrounded by an annular zone characterized by positive dT/dt. As previously explained, the central region is caused by the impinging trailing jet while the annular zone is due to the induction of the vortex ring. The main difference between the two cases is the extent of the external annular region. In this case the annular region is less wide because it is affected by the presence of a second vortex ring (generated in the previous period) which is located at r/D equal to about 3.5. This latter vortex ring has an opposite influence on this region as it induces a downwash component.

The temperature time derivatives of the last case ($32Hz$, i.e. $Sr = 0.16$) reveal the same characteristics of the other cases but a much lower extent of the annular region. This is caused by the lower distance between the positions of the two subsequent vortex rings. Indeed this distance scales with the stroke length (i.e. with the Strouhal number) because the convective velocity of vortex ring decreases with the stroke length [24].

For the $16Hz$ case ($Sr = 0.08$), six instantaneous Nusselt number maps (covering one full period) are here reported in Figure 8. While a vortex ring is present at about 4 diameters from the jet axis, the following one impinges the plate and broadens radially. For all the tests, the results in terms of instantaneous Nusselt number obtained from the balance equation on the heated thin foil (Eq. 1) are reported in the Supplementary material as movie 1 ($8Hz$, i.e. $Sr = 0.04$), movie 2 ($16Hz$, i.e. $Sr = 0.08$) and movie 3 ($32Hz$, i.e. $Sr = 0.16$). To solve the energy balance the temperature maps have been filtered with both POD and polynomial filter. The sequences clearly present a strong spatial and temporal coherence, thus assessing the proposed methodology as a powerful tool for turbulent convective heat transfer investigations.
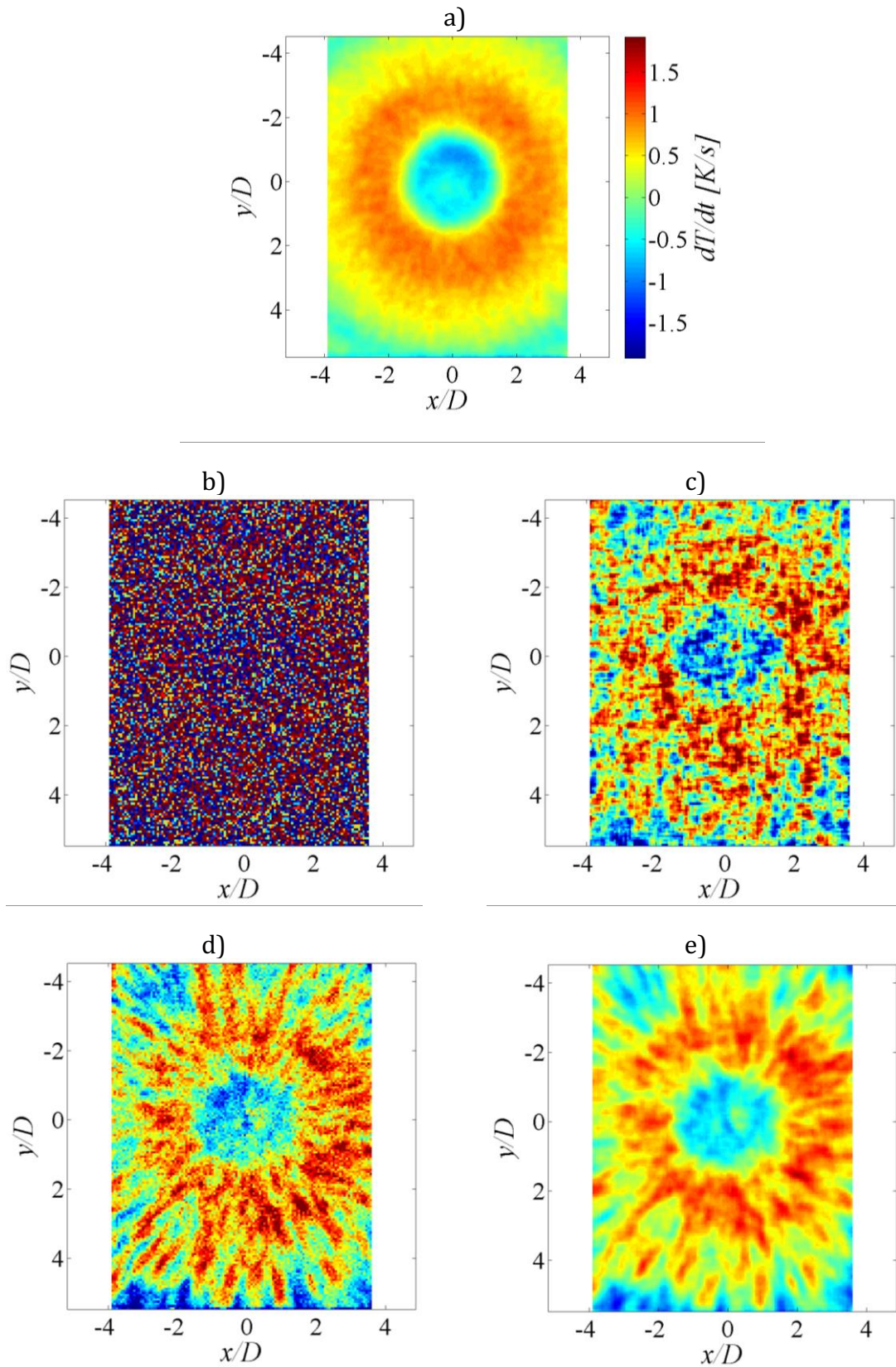
Figure 5 Time derivative of temperature maps for 8Hz case: a) phase average, b) instantaneous raw c) instantaneous polynomial filter, d) instantaneous POD filter, e) instantaneous POD+polynomial filter. For the color scale refer to a).
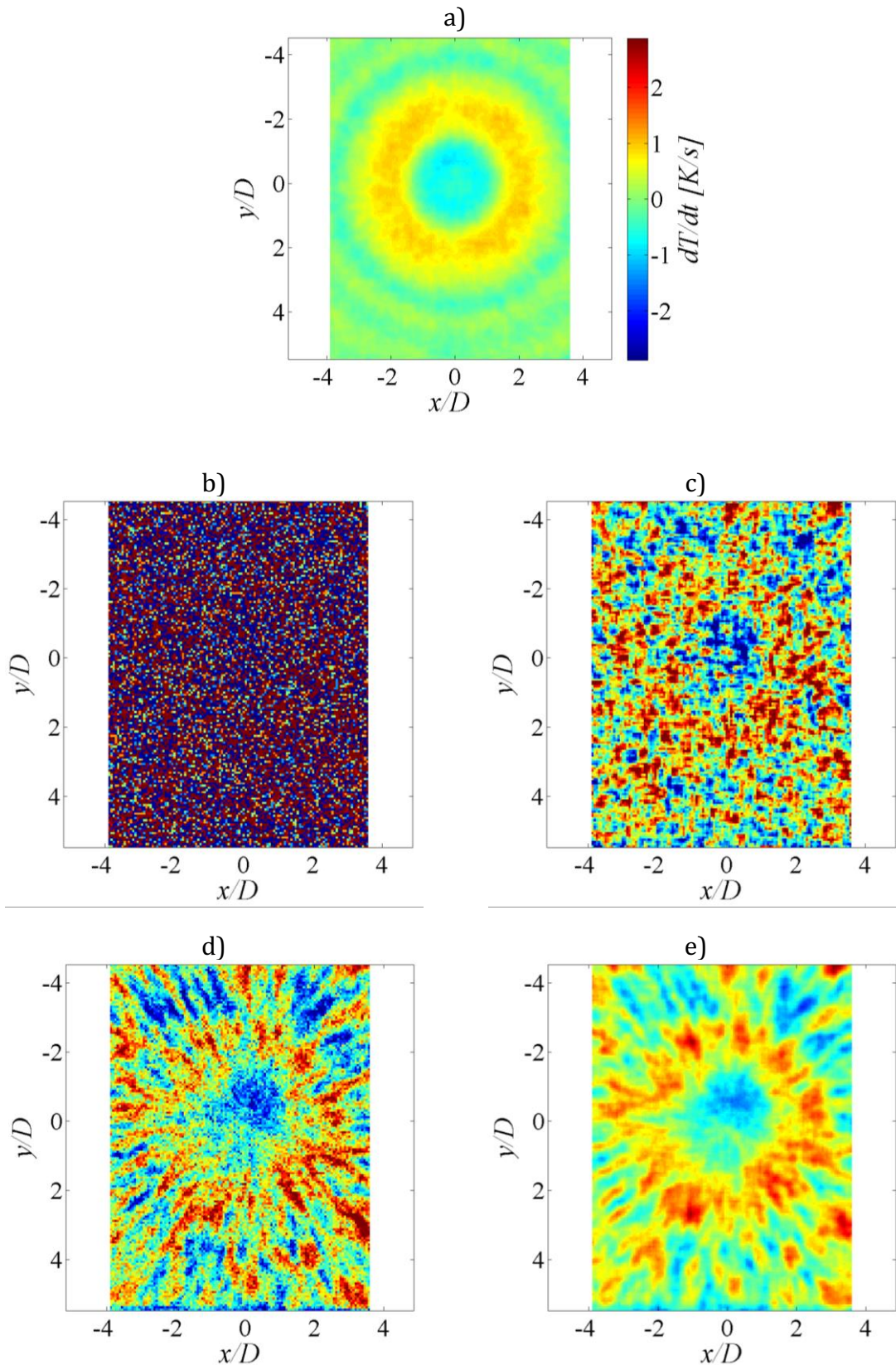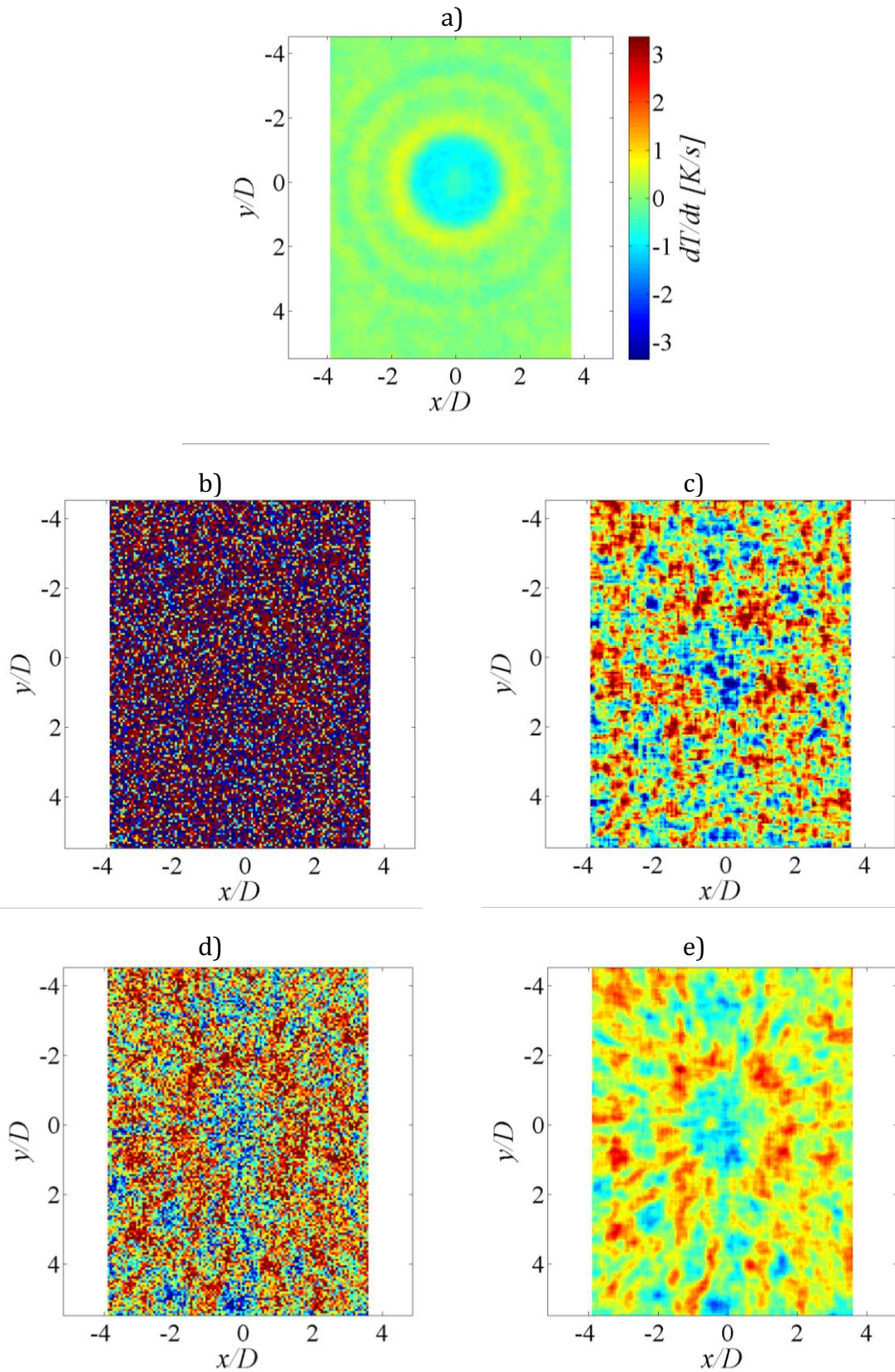
Figure 6 Time derivative of temperature maps for $16Hz$ case: a) phase average, b) instantaneous raw c) instantaneous polynomial filter, d) instantaneous POD filter, e) instantaneous POD+polynomial filter. For the color scale refer to a).

Figure 7 Time derivative of temperature maps for 32Hz case: a) phase average, b) instantaneous raw c) instantaneous polynomial filter, d) instantaneous POD filter, e) instantaneous POD+polynomial filter. For the color scale refer to a).
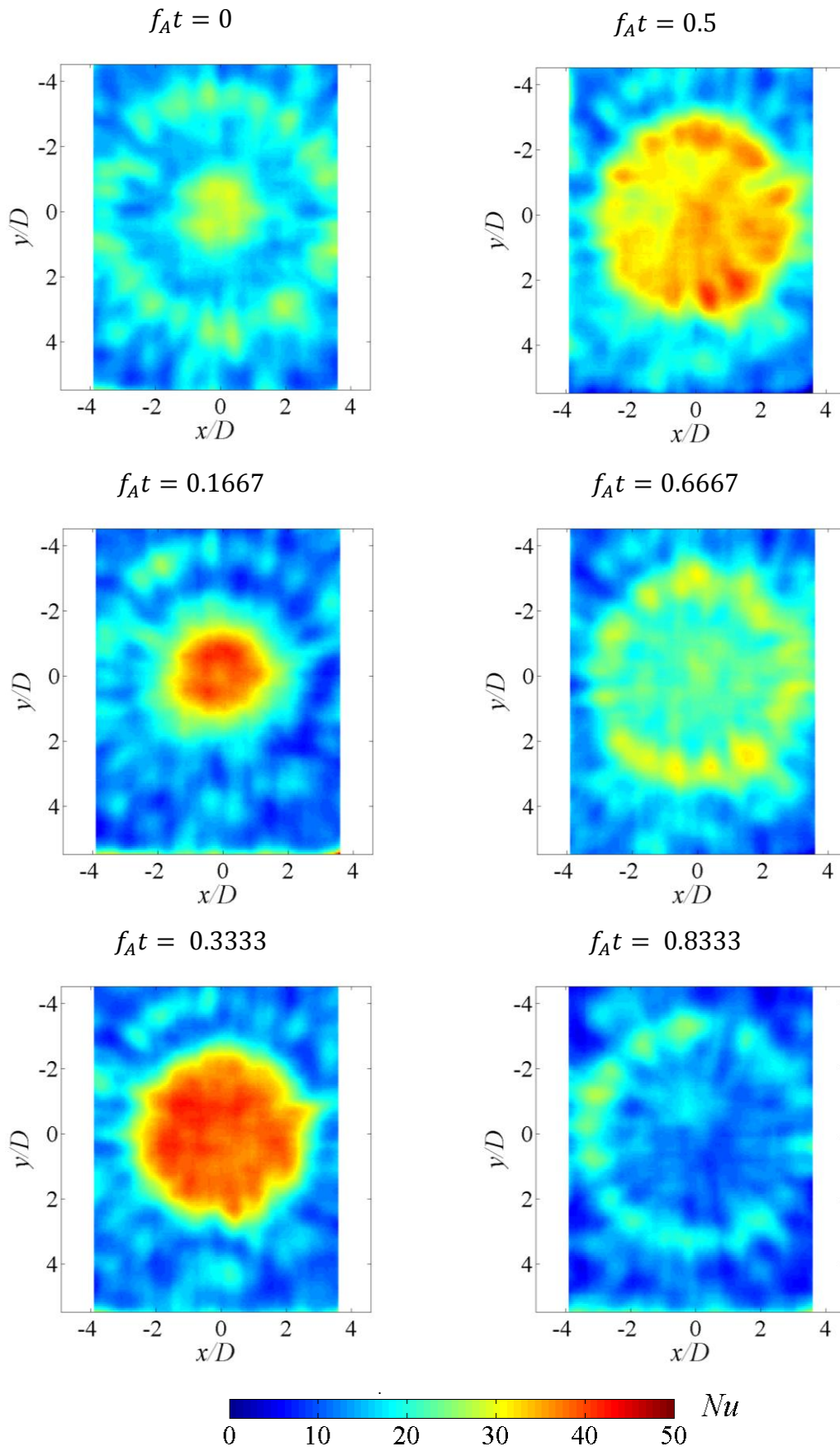
Figure 8 Instantaneous Nusselt number maps for $16Hz$ case ($Sr = 0.08$) with POD and Polynomial filter.

4 Conclusions

In this work a POD based approach is presented to reduce the noise level in temperature measurements with infrared thermography. This allows to improve dramatically the accuracy of the estimation of the unsteady term in the energy balance of a heated thin foil for turbulent convective heat transfer measurements. Since it poses the basis on statistical persistence of flow field features, the POD based filter is extremely effective in reducing spurious noise contamination on turbulent flows measurements. While this assertion is widely accepted in velocity field measurements, here it is applied and demonstrated for the first time in heat transfer measurement. A criterion for a-priori selection of the optimal number of modes for the low order reconstruction has been proposed and assessed. In general, the criterion has demonstrated being a useful tool, but more precision can be acquired using the scree-plot test [10], [17].

The method is demonstrated with a synthetic jet experiment, which has the advantage of providing a main temperature fluctuation at controlled frequency (thus identifiable via phase averaging) and smaller random fluctuations due to turbulence. The POD filter per se is able to reduce significantly the noise in the signal, thus unravelling heat transfer patterns which were almost completely hidden even after spatial-temporal filtering. On the downside, the POD filter does not remove focal plane array non-uniformity, thus its results need to be refined with a spatial filter. However, considering the reduced intensity of noise, less aggressive spatio-temporal filter can be used, thus reducing the modulation effects on real fluctuations.

Acknowledgments

References

[1] Carlomagno, G. M., & Cardone, G. (2010). Infrared thermography for convective heat transfer measurements. Experiments in fluids, 49(6), 1187-1218.

[2] Carlomagno, G. M., & Ianiro, A. (2014). Thermo-fluid-dynamics of submerged jets impinging at short nozzle-to-plate distance: a review. Experimental thermal and fluid science, 58, 15-35.

[3] Hetsroni, G., & Rozenblit, R. (1994). Heat transfer to a liquid—solid mixture in a flume. International Journal of Multiphase Flow, 20(4), 671-689.

[4]   Sanmiguel Vila, C., Discetti, S., Carlomagno, G. M., Astarita, T., & Ianiro, A. (2016). On the onset of horizontal convection. International Journal of Thermal Sciences, 110, 96-108.

[5]   Greco, C. S., Ianiro, A., & Cardone, G. (2014). Time and phase average heat transfer in single and twin circular synthetic impinging air jets. International Journal of Heat and Mass Transfer, 73, 776-788.

[6]   Nakamura, H., & Yamada, S. (2013). Quantitative evaluation of spatio-temporal heat transfer to a turbulent air flow using a heated thin-foil. International Journal of Heat and Mass Transfer, 64, 892-902.

[7]   Yamada, S., & Nakamura, H. (2016). Construction of 2D-3C PIV and high-speed infrared thermography combined system for simultaneous measurement of flow and thermal fluctuations over a backward facing step. International Journal of Heat and Fluid Flow.

[8]   Nakamura, H. (2009). Frequency response and spatial resolution of a thin foil for heat transfer measurements using infrared thermography. International Journal of Heat and Mass Transfer, 52(21), 5040-5045.

[9]   Astarita, T., & Carlomagno, G. M. (2012). Infrared thermography for thermo-fluid-dynamics. Springer Science & Business Media.

[10]   Raiola, M., Discetti, S., & Ianiro, A. (2015). On PIV random error minimization with optimal POD-based low-order reconstruction. Experiments in Fluids, 56(4), 1-15.

[11]   Berkooz, G., Holmes, P., & Lumley, J. L. (1993). The proper orthogonal decomposition in the analysis of turbulent flows. Annual review of fluid mechanics, 25(1), 539-575.

[12]   Pastuhoff, M., Yorita, D., Asai, K., & Alfredsson, P. H. (2013). Enhancing the signal-to-noise ratio of pressure sensitive paint data by singular value decomposition. Measurement Science and Technology, 24(7), 075301.

[13]   Levesque P, Brémond P, Lasserre JL, Paupert A and Balageas DL (2005) Performance of FPA IR cameras and their improvement by time, space and frequency data processing. Part I: Intrinsic characterization of the thermographic system. QIRT J., Vol. 2, pp. 97-112.

[14]   Fahl, M. (2000). Trust-region methods for flow control based on Reduced Order Modeling (Doctoral dissertation, Ph. D. thesis, Trier university).

[15]   Sirovich, L.(1987) Turbulence and the dynamics of coherent structures: I, II, III, Q. Appl. Math. 45:561-590.

[16]   Pope, S. B. (2001). Turbulent flows. Cambridge University Press.

[17]   Cattell, R.B. (1966) The scree test for the number of factors. Multivar.Behav. Res. 1: 245-276.

[18]   Greco, C. S., Ianiro, A., Astarita, T., & Cardone, G. (2013). On the near field of single and twin circular synthetic air jets. International Journal of Heat and Fluid Flow, 44, 41-52.

[19]   Smith, B. L., & Glezer, A. (1998). The formation and evolution of synthetic jets. Physics of Fluids (1994-present), 10(9), 2281-2297.

[20] de Luca, L., Girfoglio, M., & Coppola, G. (2014). Modeling and experimental validation of the frequency response of synthetic jet actuators. AIAA Journal, 52(8), 1733-1748.

[21] Greco, C.S., Cardone, G., Soria, J. (2016). On the behaviour of impinging zero-net-mass-flux jets. Journal of Fluid Mechanics, doi:10.1017/jfm.2016.703.

[22] Mooney, J. M., Sheppard, F. D., Ewing, W. S., Ewing, J. E., & Silverman, J. (1989). Responsivity nonuniformity limited performance of infrared staring cameras. Optical Engineering, 28(11), 281151-281151.

[23] Carlomagno, G. M., Discetti, S., & Astarita, T. (2011). Experimental assessment of a new heat flux sensor for measuring convective heat transfer coefficients. Quantitative InfraRed Thermography Journal, 8(1), 37-49.

[24] Shuster, J. M. & Smith, D. R. (2007). Experimental study of the formation and scaling of a round synthetic jet. Physics of Fluids 19(4), 045109.